




## Molecular modelling on SARS-CoV-2 papain-like protease: an integrated study with homology modelling, molecular docking, and molecular dynamics simulations

A. Arwansyah, A.R. Arif, I. Ramli, I. Kurniawan, S. Sukarti, M. Nur Alam, I. Illing, A. Farid Lewa & B. Manguntungi

To cite this article: A. Arwansyah, A.R. Arif, I. Ramli, I. Kurniawan, S. Sukarti, M. Nur Alam, I. Illing, A. Farid Lewa & B. Manguntungi (2021): Molecular modelling on SARS-CoV-2 papain-like protease: an integrated study with homology modelling, molecular docking, and molecular dynamics simulations, SAR and QSAR in Environmental Research, DOI: [10.1080/1062936X.2021.1960601](https://doi.org/10.1080/1062936X.2021.1960601)

To link to this article: <https://doi.org/10.1080/1062936X.2021.1960601>

 View supplementary material 

 Published online: 16 Aug 2021.

 Submit your article to this journal 

 View related articles 

 View Crossmark data 



# Molecular modelling on SARS-CoV-2 papain-like protease: an integrated study with homology modelling, molecular docking, and molecular dynamics simulations

A. Arwansyah<sup>1</sup>, A.R. Arif<sup>2</sup>, I. Ramli<sup>3</sup>, I. Kurniawan<sup>4,5</sup>, S. Sukarti<sup>6</sup>,  
M. Nur Alam<sup>7</sup>, I. Illing<sup>8</sup>, A. Farid Lewa<sup>9</sup> and B. Manguntung<sup>9</sup>

<sup>1</sup>Department of Chemistry, Faculty of Science, Cokroaminoto University of Palopo, Palopo, Indonesia; <sup>2</sup>Department of Chemistry, Faculty of Mathematics and Natural Sciences, Hasanuddin University, Makassar, Indonesia; <sup>3</sup>Department of Physics, Faculty of Science, Cokroaminoto University of Palopo, Palopo, Indonesia; <sup>4</sup>School of Computing, Telkom University, Bandung, Indonesia; <sup>5</sup>Research Center of Human Centric Engineering, Telkom University, Bandung, Indonesia; <sup>6</sup>Department of Nutrition, Poltekkes Kemenkes Palu, Palu, Indonesia; <sup>7</sup>Department of Biotechnology, Faculty of Biotechnology, Sumbawa University of Technology, Sumbawa, Indonesia

## ABSTRACT

SARS-CoV-2 PLpro was investigated as a therapeutic target for potent antiviral drugs due to its essential role in not only viral replication but also in regulating the inborn immune response. Several computational approaches, including homology modelling, molecular docking, and molecular dynamics (MD) studies, were employed to search for promising drugs in treating SARS-CoV-2. Eighty-one compounds, sub-structurally similar to the antiviral drug, were used as potential inhibitors of PLpro. From our results, three complexes containing the ligands with Pubchem IDs: 153012995, 12149203, and 123608715 showed lower binding energies than the control (Ritonavir), indicating that they may become promising inhibitors for PLpro. MD was performed in a water solvent to validate the stability of the three complexes. All complexes achieved stable structure during the simulation as no significant fluctuations were observed in the validation parameters. Moreover, the binding energy for each complex was estimated using the MM-GBSA method. Complex 1 was the most stable structure based on the lowest binding energy score and its structure remained in a similar cavity with the docket snapshot. Based on our studies, three ligands were assumed to be potential inhibitors. The ligand of complex 1 may become the most promising antiviral drug against SARS-CoV-2 targeting PLpro.

## ARTICLE HISTORY

Received 11 May 2021  
Accepted 21 July 2021

## KEYWORDS

SARS-CoV-2 PLpro;  
promising antiviral drug;  
homology modelling;  
molecular docking; MD  
simulations

## Introduction

The novel severe acute respiratory syndrome coronavirus 2 (SARS-CoV-2), known as Covid-19, has become a global emergency disease since more than 125 million confirmed cases (update March 24th, 2021) from around 235 world countries have been reported to World Health Organization (WHO) [1]. The first case of Covid-19 was

**CONTACT** A. Arwansyah ✉ [arwansyah@uncp.ac.id](mailto:arwansyah@uncp.ac.id); A.R. Arif ✉ [arrahman.arif@unhas.ac.id](mailto:arrahman.arif@unhas.ac.id)  
Supplemental data for this article can be accessed at: <https://doi.org/10.1080/1062936X.2021.1960601>

announced from Wuhan city seafood market, China, and declared a global pandemic on March 11th, 2020. SARS-CoV-2 can affect pneumonia that initiates acute respiratory failure in humans [2–5]. Therefore, molecular investigation on the constituent of the virus structure, including searching for a potent antiviral drug or vaccine, needs to work as soon as possible due to the dangerous impact on human life caused by SARS-CoV-2 infection.

SARS-CoV-2, classified as Betacoronavirus (Riboviria), is a positive-sense single-strand RNA (ss-RNA) virus with a genome size range of about 27 to 34 kilobases [6–10]. SARS-CoV-2, including severe acute respiratory syndrome (SARS) and middle east respiratory syndrome (MERS) viruses, grouped as the coronaviruses, are recognized to attack the respiratory region, and gastrointestinal infections to the human [11–15]. Several species can be a reservoir of the coronavirus family, and some countries, including China, have reported that bats are the main reservoir of SARS-CoV-2. This virus can be spread from human to human via respiratory droplets from coughs, sneezes and by touching contaminated objects [16–20].

At present, the developments to the SARS-CoV-2 therapy have significantly increased for treatment or even preventing the virus attack. Several vaccines such as Pfizer/BioNTech, AstraZeneca, Sinovac, Moderna have been approved and consumed by people in various countries [21–23]. Those vaccines' efficacy and safety against the virus have been announced after the clinical test to the communities. Side effects of vaccines have also been presented, including feeling tired, a severe allergic reaction, headache, chills, and mild fever. Another treatment utilized for SARS-CoV-2 patients is to consume existing antiviral drugs such as Favipirafir, Remdesivir, Ribavirin, Sofosbuvir to prevent the virus gain [24–28]. Thus, further investigation on structurally similar compounds with these antiviral drugs is also required to find the alternative antiviral drug with effective therapeutic treating SARS-CoV-2 and event SARS-CoV-2 mutation variants.

To inhibit the virus life cycle, some proteins such as main protease, spike protein, and RNA-dependent RNA polymerase (RdRp) have been investigated as main targets for blocking viral infection [29–32]. Another concern of the antiviral target is a papain-like protease (PLpro) due to its essential role in virus existence. Several research groups have investigated the structure of SARS-CoV-2 PLpro by X-ray analysis [33–35]. PLpro is a protein encoded by the ORF1ab gen whose primary structures consist of ubiquitin-like, thumb, palm, and finger segments. This protein involves in viral replication and controlling inborn immune response [34,36,37]. To treat SARS-CoV-2, Ritonavir, one of a protease inhibitor with activity against Human Immunodeficiency Virus Type 1 (HIV-1), has been used to inhibit PLpro action in the replication process. Ritonavir inhibits the HIV viral proteinase enzyme that normally cleaves genes of gag and pol. These genes correlate to the structural and replicative protein from major HIV genes such as nucleocapsid, HIV reverse transcriptase, ribonuclease H, integrase, and protease 1. From this action, Ritonavir is applied to cleave the polyproteins synthesized by viral proteases of SARS-CoV-2 in which prevents the further biological mechanism of the virus on transcription and replication of viral RNA [38,39]. Hence, inhibition of the PLpro protein with an antiviral drug can provide advantages for not only to prevent the growth of a new virus but also to terminate the regulation of signalling coordination in an infected cell.

In experimental research, PLpro protein as a therapeutic target against SARS-CoV-2 has been reported. In the paper presented by Gao and co-workers, peptide inhibitor

GRL0617 was employed to investigate its inhibitory action to SARS-CoV-2 PLpro [40]. The authors revealed that the inhibitory value of IC<sub>50</sub> of  $2.2 \pm 0.3 \mu\text{mol/L}$  was obtained after testing to PLpro. This finding suggested that the peptide inhibitor GRL0617 might become a potential antiviral drug for treating SARS-CoV-2. Meanwhile, in the computational investigation, SARS-CoV-2 PLpro was targeted to examine 21 antiviral, antifungal, and anticancer compounds by molecular docking method [41]. Among them, Neobavaisoflavone was assumed to become a potent antiviral drug due to the lowest energy score and binding to the crucial catalytic triad of SARS-CoV-2 PLpro.

In this present study, we investigate the potential of the sub-structurally similar compounds with Ritonavir deposited from Pubchem database as promising antiviral drugs for SARS-CoV-2 by several computational approaches. Homology modelling was carried out to obtain a tertiary structure model of the SARS-CoV-2 PLpro. Then, molecular docking was performed to find the antiviral drugs' binding site into the catalytic site of PLpro protein using a particular searching algorithm and scoring functions [42–44]. This method is commonly used to design a new drug by providing valuable initial evidence before investigating experimental research [45–48]. Further, to confirm the complex obtained by docking is stable in a water solvent, we performed all-atom molecular dynamics (MD) simulation on selected drugs in a complex with PLpro. The binding energy was estimated to find the most stable complex from the trajectories of MD simulations. A combination of computational approaches, including homology modelling, molecular docking, and MD studies, was expected to be suited to find a new potent antiviral drug as the valuable treatment against SARS-CoV-2 targeting PLpro.

## Materials and methods

### *Homology modelling and evaluation*

The sequence protein of SARS-CoV-2 papain-like protease (SARS-CoV-2 PLpro) was retrieved from the National Center for Biotechnology Information (NCBI) database (PDB: 7E35\_A, GI: 2007122772). The FASTA file was extracted to search for the similarity of the protein sequence using the Basic Local Alignment Search Tool (pBLAST). A total of 33 sequences were obtained, which provided > 30% similarity with PLpro sequence input. We selected the top 10 PDB files, i.e. 7D6H, 6XAA, 6XA9, 7CJM, 6WRH, 7D47, 6YVA, 7CJD, 6WUU, and 6W9C, with similarity percentage > 99% of PLpro to determine which structure will be applied as a reference template. Using Modeller v10.0 program packages [49], the sequence identity comparison and weighted pair group average clustering analysis were used to choose a reference template from those PDB structures. Then, homology modelling using a similar program (Modeller v10.0) was performed on the reference template. Ten structures were predicted, and the best possible structure of those structures was chosen based on the highest value of discrete optimized protein energy (DOPE) score. The best-predicted model was aligned to the reference template to confirm the similarity of the protein sequence. The detailed information of the database and software used in this present investigation is given in Table S1.

## Molecular docking

In the present investigation, we performed a molecular docking simulation to obtain the binding pocket of the ligand into the receptor's catalytic site. The AutoDock Vina package developed by Trott and co-workers was utilized to perform molecular docking on the ligand-receptor complex [50]. The promising drugs as ligand molecules were retrieved from the PubChem database (<https://pubchem.ncbi.nlm.nih.gov/>). Eighty-one compounds that have sub-structurally similar drug with Ritonavir were retrieved from the database. The drug candidates were collected as follows: all compounds were downloaded and saved to SDF extension. Then, the SDF files were converted to PDBQT format by Open Babel 2.4.1 program packages [51]. The charges of the molecules were automatically added as the program default. To prepare the protein target, the structure of the SARS-CoV-2 papain-like protease (SARS-CoV-2 PLpro) was taken from the protein model, which was created in [subsection 2.1](#). The hydrogen atoms and Kollman's united atom charges were inserted into the receptor. Afterwards, PDBQT formats were created for the receptor. The grid box size was set around the catalytic site of PLpro on  $52 \times 46 \times 52$  points with a grid spacing of 1.00 Å. The grid box centre was located at the coordinate (x, y, z) = (8.079, -266.256, 88.683). The exhaustiveness parameter was fixed at 100. For searching parameters, the Broyden- Fletcher-Goldfarb-Shanno (BFGS) algorithm was employed to find the binding site, including the conformation pose of the ligand into the site of the receptor. Other parameters, including energy range, random seed, etc., were computed as the default of AutoDock Vina. AutoDock Tools 1.5.6 was utilized to prepare All docking parameters [52]. The docking simulation was performed according to the similar procedure provided in our previous works [53,54].

## Molecular dynamics study

All-atom molecular dynamics simulation using Amber 16 packages was performed on the ligand in complex with the receptor [55]. This method was applied to validate the stability of the complex selected from the molecular docking after assessing the binding energy and ligand binding site in binding with the receptor. TIP3P water models [56] and  $\text{Na}^+$  ions were inserted into the cubic box size of the system. The force field parameters of ligands and receptors were determined by employing the general AMBER force field (GAFF) [57] and AMBER14 force field [58], respectively. The electrostatic interactions were computed by using the Particle Mesh Ewald (PME) [59], and the distance of the hydrogen atom was constrained by SHAKE [60] algorithms. The switching cut-off distance was set at 10 Å. The time step of 2 fs was applied for all simulations.

To perform MD simulation, the energy minimization on the system was firstly carried out. Then, the temperature was gradually increased from 0 to 300 K by performing NVT-constant for 500 ps. The temperature was kept at 300 K by using Langevin thermostat [61] and the pressure of the system was maintained at 1 atm using the isotropic position scaling algorithm. The system was equilibrated with the NPT ensemble for 250 ns, and the trajectory was saved for every 5000 steps (10 ps). CPPTRAJ tools [62] were used to analyse the trajectories of MD simulation.

We estimated the root-mean-square deviation (RMSD) of the complex to verify the stability of the ligands in binding with receptor as the following equation:

$$RMSD(t_1) = \left[ \frac{1}{M} \sum_{i=1}^N m_i \| r_i(t_i) - r_{ref,i} \|^2 \right]^{\frac{1}{2}} \quad (1)$$

where  $m_i$  is the mass of atom  $i$ ,  $N$  is the total number of atoms in the model complex,  $M$  is the total mass of all atoms, and  $r_i$  is the position of atom  $i$  at the time  $t$ , and  $r_{ref,i}$  is the positions of  $i$ -th atom in the X-ray structure, respectively.

### MM-GBSA binding energy

To estimate the binding energy of receptor-ligand complex, molecular mechanics generalized Born surface area (MM-GBSA) method was employed developed by Miller and co-workers [63]. The binding energy was estimated from the trajectories of MD simulations according to the following equation:

$$\Delta G_{binding} = -RT \ln K_i = G_{complex} - (G_{receptor} + G_{ligand}) \quad (2)$$

the energy term is calculated as follows:

$$G = E_{vdw} + E_{ele} + E_{GB} + E_{SA} \quad (3)$$

where  $E_{vdw}$ ,  $E_{ele}$ ,  $E_{GB}$ , and  $E_{SA}$  are the van der Waals, electrostatic, general Born solvation and surface area energies, respectively.

## Results and discussion

### Protein modelling and structure prediction

Because the X-ray structures found in the PDB database are not always complete, the homology modelling approach is often applied to carry out the comparative modelling of protein structure. To obtain the tertiary structure of SARS-CoV-2 papain-like protease (SARS-CoV-2 PLpro), some protocols were applied as previously described. A total of 33 protein sequences obtained by pBLAST were saved in the FASTA extension (See supplementary file 2). The top 10 PDB files, including 7D6H, 6XAA, 6XA9, 7CJM, 6WRH, 7D47, 6YVA, 7CJD, 6WUU, and 6W9C, were screened to find a reference template of PLpro. Using the homology method performed by Modeller v10.0 program packages, we obtained the sequence identity comparison for each PDB listed in Table S2. This identity comparison was utilized to calculate the weighted pair group average clustering analysis shown in Figure S1 of supplementary file 1. From this figure, the sequence identity, including the relation between SARS-CoV-2 PLpro saved in the PDB database, was presented. Further, a reference template could be selected based on the crystallographic resolution from this figure. 7D6H and 6WRH have better structures with a similar crystallographic resolution of 1.6 Å. In this case, 7D6H was selected as the reference template since it has a better crystallographic resolution and higher similarity of 100% with SARS-CoV-2 PLpro from the NCBI database (PDB: 7D7T\_A, GI: 1820435677). Thus, this template structure was used for homology modelling to create a protein model of SARS-CoV-2 PLpro. Using the 7D6H structure as a template, we generated 10 protein models. Three dimensional (3D) structure of SARS-CoV-2 PLpro was selected with the lowest DOPE score. As summarized in Table S3, model 3 was chosen for SARS-CoV-2 PLpro due to the lowest DOPE score of

35872.710, and the DOPE per residue score between PLpro template and model 3 was analysed (Figure S2). The trend graph of those scores looked identical in shape. This finding indicated that created model was an almost similar structure to the reference template. Therefore, this protein model was extracted to align the sequence of amino acid residues (Figure S3). Four gaps of amino acids were observed for template structure compared to the PLpro model. In the protein model, 4 residues, including GLY1, PRO2, GLY3, and SER4, were filled to those gaps. Our protein model by homology modelling might improve the tertiary structure of SARS-CoV-2 PLpro due to filling missing amino acids in the initial sequences of PLpro. The tertiary structure of the SARS-CoV-2 PLpro model using reference template 7D6H is shown in Figure S4. In SARS-CoV-2 PLpro, the protein's catalytic triad consists of some residues such as SER111, HIS272, and ASP286, respectively [40]. After homology modelling, those residues are changed to the sequence numbers: SER116, HIS277, and ASP291 in the PLpro model. These residues are important sites for binding a ligand into the moiety of PLpro. Therefore, a potent ligand that can bind to those sites is assumed to have an inhibitory action for treating SARS-CoV-2.

### **Molecular docking**

In the previous subsection, we have created the tertiary structure of the SARS-CoV-2 PLpro model from the template structure of PDB: 7D6H. To perform molecular docking simulation, the created PLpro (receptor) model was utilized as a primary target receptor for drug candidates against SARS-CoV-2. Meanwhile, 81 ligands treated as anti-SARS-CoV-2 were retrieved from the PubChem database. The possibility of ligand in complex to the site of the receptor was achieved when the complex has the negative binding energy. From our simulation, 81 complexes were obtained with various binding energies, listed in Table 1. All ligands might bind to the receptor since all binding energy scores were in negative values. This result indicated that all ligands could make a complex with the receptor. Also, we see the top 3 complexes having the ligands with PubChem IDs: 153012995, 12149203, and 123608715 (Figure 1) showed lower binding energies with the values of  $-6.6$ ,  $-6.6$ , and  $-6.4$  kcal/mol, respectively. These complexes revealed higher binding energy than Ritonavir as control positive (PubChem ID: 492405) with the binding energy of  $-5.7$  kcal/mol. This finding suggested that those 3 ligands could become promising inhibitors for SARS-CoV-2 PLpro and might easily bind to the receptor's catalytic region to make a ligand-receptor complex. Therefore, we selected and extracted the snapshot structure of the ligands to analyse the molecular interactions such as hydrogen bond and hydrophobic interaction between ligand and receptor [64,65]. For further analysis, the complexes containing those 3 ligands are written as complexes 1, 2, and 3, respectively.

Figure 2 shows the binding site and position pose of the selected ligands in complex with the receptor. From this figure, hydrogen bond and hydrophobic interactions participated in the binding of ligand to the receptor. The particulars of hydrogen bonds for all complexes are summarized in Table 2. We show that the ligand of complex 1 contribute to hydrogen bonds with residues TRP111, SER116, THR270, and LYS277 of the receptor. For complex 2, the ligand participate in hydrogen bonds with residues GLU268, THR270, and LYS279. In complex 3, the hydrogen bonds are formed between ligand and residues of THR270 and THR279. Meanwhile, for control (Ritonavir), the hydrogen bonds are formed between the side chain of ligand and residues GLU268, THR270, LYS279, and ASP291 of

**Table 1.** The binding energies (BE) of ligands in complex with the receptor (SARS-CoV-2 PLpro) obtained by molecular docking. The PubChem ID: 392622 denotes the Ritonavir drug, which was used as a positive control with the binding energy of  $-5.7$  kcal/mol.

No.	PubChem CID	BE (kcal/mol)	No.	PubChem CID	BE (kcal/mol)	No.	PubChem CID	BE (kcal/mol)
1	153012995	-6.6	29	22863118	-5.1	57	5076	-4.8
2	12149203	-6.6	30	22878492	-5.1	58	9853294	-4.8
3	123608715	-6.4	31	482947	-5.1	59	5271820	-4.7
4	151552230	-6.1	32	482963	-5.1	60	60126661	-4.7
5	90333440	-5.9	33	60954	-5.1	61	60126718	-4.7
6	15850559	-5.9	34	17838568	-5.0	62	69758109	-4.7
7	60126655	-5.8	35	10395099	-5.0	63	69760543	-4.7
8	44371018	-5.8	36	22862935	-5.0	64	22862857	-4.7
9	90825158	-5.7	37	22863119	-5.0	65	42638007	-4.7
10	22862965	-5.7	38	22863125	-5.0	66	60126645	-4.6
11	22662837	-5.6	39	44371228	-5.0	67	70023974	-4.6
12	70022741	-5.6	40	482955	-5.0	68	22862961	-4.6
13	22863127	-5.6	41	482957	-5.0	69	22863031	-4.6
14	16760215	-5.5	42	515824	-5.0	70	44325718	-4.6
15	44371020	-5.5	43	151085868	-4.9	71	44371241	-4.6
16	22862923	-5.4	44	69760166	-4.9	72	149566833	-4.5
17	482937	-5.4	45	70023764	-4.9	73	70023775	-4.5
18	22867769	-5.3	46	18624599	-4.9	74	90339326	-4.5
19	482943	-5.3	47	22862817	-4.9	75	44371081	-4.5
20	15850558	-5.2	48	22878493	-4.9	76	482948	-4.5
21	44371170	-5.2	49	455315	-4.9	77	482954	-4.5
22	44371171	-5.2	50	69875991	-4.8	78	25059201	-4.4
23	482960	-5.2	51	70023763	-4.8	79	42637793	-4.0
24	482961	-5.2	52	22862827	-4.8	80	22863023	-3.9
25	22662766	-5.1	53	22868003	-4.8	81	42637792	-3.8
26	69921403	-5.1	54	23389094	-4.8	82	392622 (Control)	-5.7
27	22862838	-5.1	55	4074035	-4.8			
28	22863035	-5.1	56	42637730	-4.8			

receptor. From these results, each complex might become stable structures since the hydrogen bonds were coordinated between ligand and receptor. Further, as previously mentioned, a promising drug that can bind to the catalytic site of PLpro, which includes residues SER116, HIS277, and ASP291, is supposed to have an inhibitory action due to its biological function for viral replication [40]. From our docking simulation, ligand 1 bound with residues SER116 and HIS277 of PLpro. This result suggests that the ligand in complex 1 might become a promising drug against SARS-CoV-2 due to its binding to the catalytic site of PLpro. In complexes 2 and 3, these ligands are bound with LYS279. This residue is near a catalytic site of LYS277, which indicates that the conformation structure of the catalytic site may change because of those ligands, and affecting the PLpro cannot make a new viral during the replication process. Meanwhile, the control bound with one of the catalytic sites of PLpro (ASP291), confirming Ritonavir is a drug that can inhibit PLpro activity. Therefore, from our finding, all selected ligands might have potential drugs against SARS-CoV-2 targeting PLpro.

Due to the crucial part for the stability of the binding site between ligand and receptor, we also identified the hydrophobic interactions of selected ligands with involved residues of PLpro by using LigPlot v.4.5.3 packages [66]. The two-dimension (2D) of the hydrophobic interactions for each complex is provided in Figure 3. The ligand of complex 1 makes hydrophobic interactions with residues of the receptor such as GLU166, SER116, TRP111, HIS277, LEU294, ASP291, GLU268, LYS279, THR270, GLY271, ASN114, GLY276, GLY168,



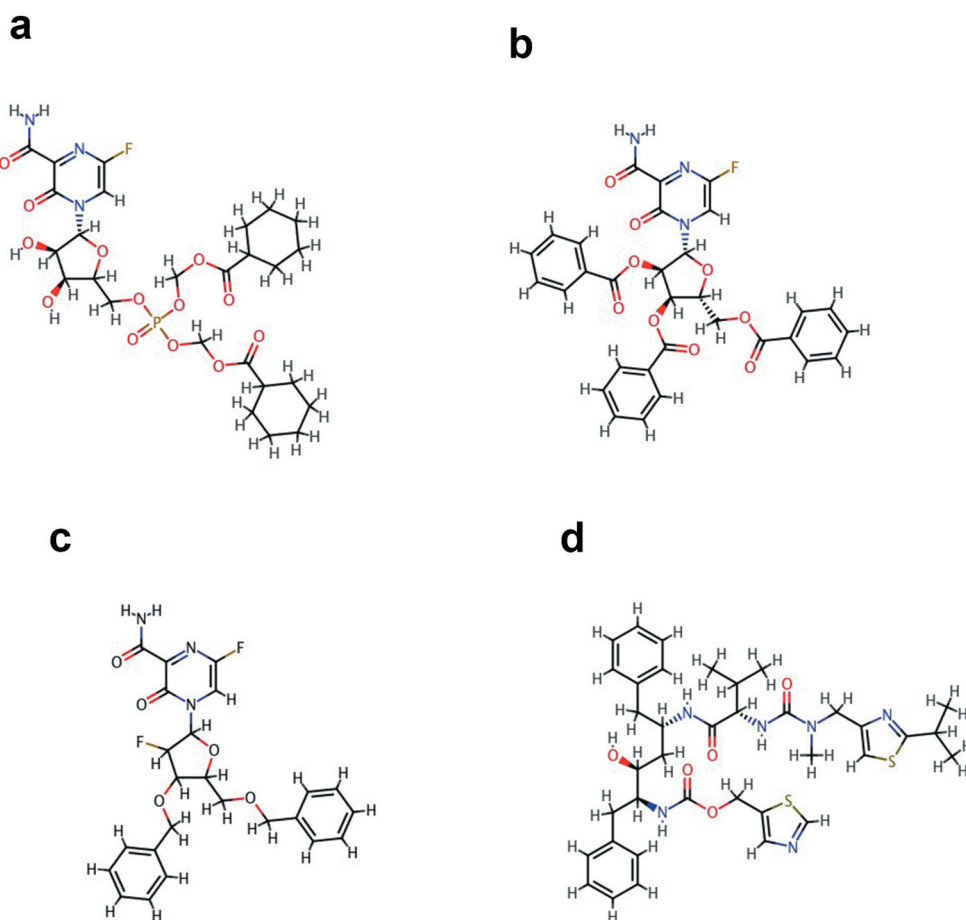


**Figure 1.** The chemical structure of selected compounds from molecular docking (a) compound 153012995, (b) compound 12149203, (c) compound 123608715, and (d) compound 392622 (Ritonavir as a control).

TYR117, LEU167, and THR270. In complex 2, the hydrophobic interaction is shown by the ligand's interaction with residues of the receptor, which include GLY271, THR270, GLU268, LYS279, ASP291, LEU294, TRP111, HIS277, GLY276, and GLY271. For complex 3, hydrophobic interactions are formed between ligand and residues GLU268, THR270, HIS277, TRP111, LEU294, ASP291, LYS279. Meanwhile, the control contributes to hydrophobic interaction with residues CYS289, THR296, TRP111, GLY276, HIS277, LYS279, THR270, GLU268, ASP291, and LEU294, respectively. From these results, we observe that the ligand of complexes 2 and 3 participate in hydrophobic interactions with residues of the catalytic site of PLpro, i.e. SER116, HIS277, and ASP291. These results imply that the hydrophobic interaction also contributes to the stability of ligand in the moiety of the receptor.

### **Drug-likeness of selected compounds**

The pharmacokinetic properties in relation to the ADME (absorption, distribution, metabolism, and excretion) of the selected compounds were analysed using SwissADME online

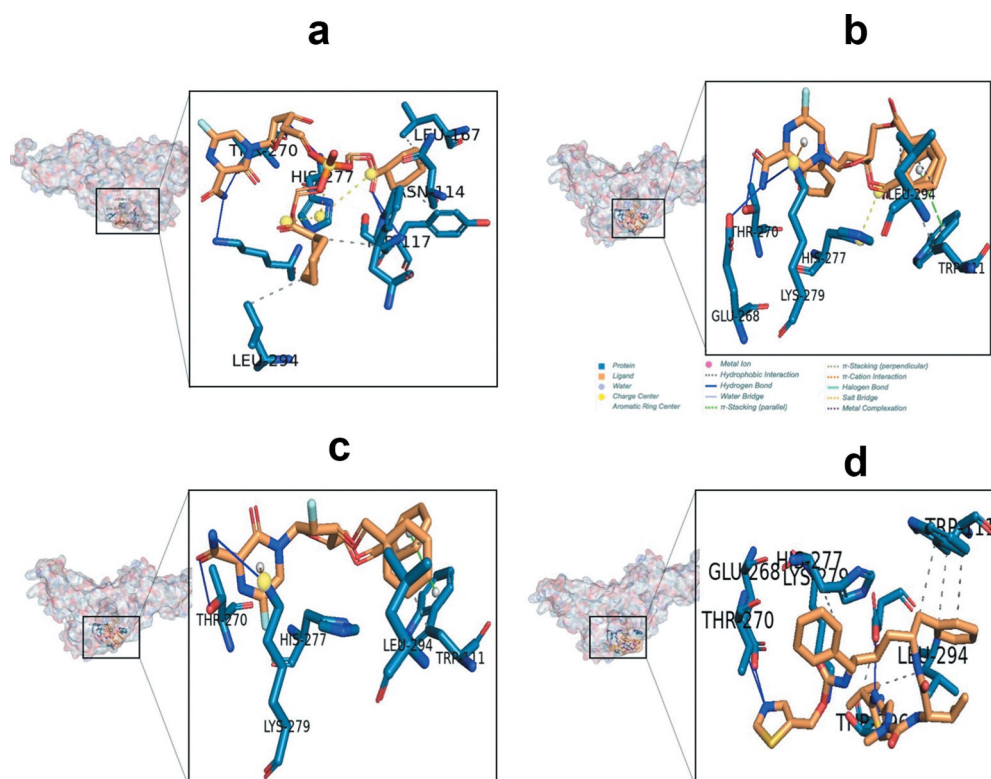


**Figure 2.** The binding mode of the ligand into the site of the receptor (SARS-CoV-2 PLpro). (a) complex 1, (b) complex 2, and (c) complex 3, and (d) control. The conformation pose of each complex is visualized by PLIP program [64] combined with Pymol v 2.3 program packages [65].

**Table 2.** Hydrogen bonds of selected ligands in complex with receptor.

Complex	Residue	AA	Distance H-A (Å)	Distance D-A (Å)	Donor Angle	Donor Atom	Acceptor Atom
Complex 1	111	TRP	2.00	2.94	152.36	1765 (N)	5047 (O2)
	116	SER	3.00	3.85	141.23	1828 (N)	5047 (O2)
	270	THR	2.16	2.71	114.49	5041 (O3)	4223 (O3)
	270	THR	2.13	2.90	137.05	4216 (O3)	5035 (N)
	270	THR	2.04	2.90	141.14	5035 (N)	4216 (O3)
	277	HIS	3.57	3.99	107.14	4300 (N)	5041 (O3)
Complex 2	277	LYS	2.97	3.76	135.03	4355 (N)	5035 (O3)
	268	GLU	2.02	2.92	146.06	5031 (N)	4186 (O2)
	270	THR	2.36	3.25	157.86	4216 (O3)	5034 (O2)
Complex 3	279	LYS	2.81	3.62	136.74	4355 (N)	5031 (N)
	270	THR	2.18	3.09	161.26	4216 (O3)	5035 (O2)
Control	279	LYS	2.89	3.76	143.09	4355 (N)	5032 (N)
	268	GLU	2.09	3.08	161.62	5066 (N)	4186 (O2)
	270	THR	2.12	3.03	161.83	4216 (O3)	5066 (N)
	279	LYS	2.72	3.14	105.17	4355 (N3)	5062 [O3]
	291	ASP	2.02	2.95	150.27	5021 (N)	4552 (O2)

tool (<http://www.swissadme.ch/index.php>). The SMILES format of compounds (See Table S4) for the input file was located to the "entry line." The analysis of ADME was performed by clicking "Run" menu, and the pharmacokinetic properties of the compounds are

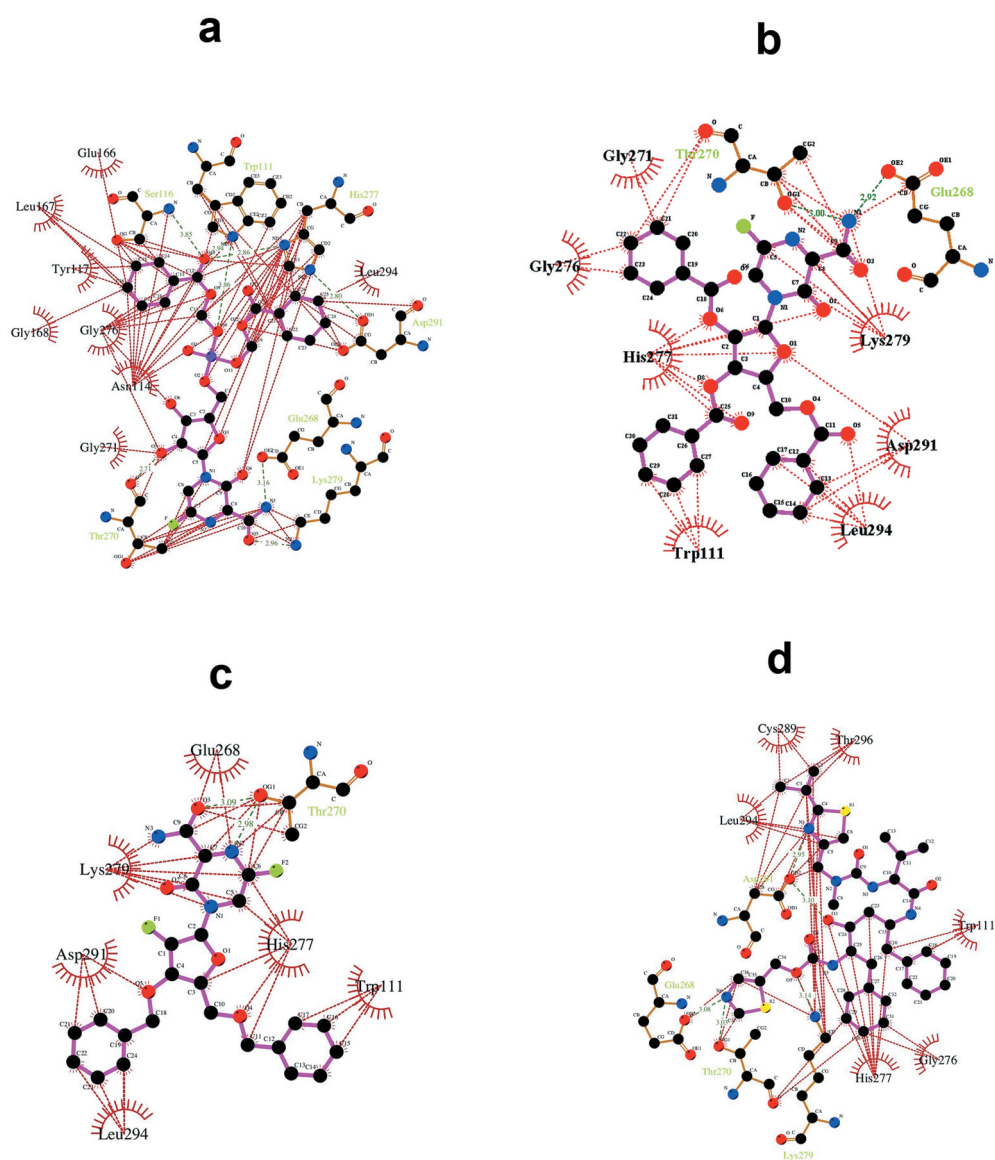


**Figure 3.** Hydrophobic interaction of the ligand in binding with receptor (SARS-CoV-2 PLpro). (a) complex 1, (b) complex 2, and (c) complex 3, and (d) control.

generated in the output display of the online tool. Lipinski's rule of five (molecular weight  $< 500$  Daltons,  $\log P \leq 5$ ,  $\leq 5$  hydrogen bond donors,  $\leq 10$  hydrogen bond acceptor, and  $PSA < 140 \text{ \AA}^2$ ) is mostly used to consider in optimal drug-likeness behaviour. According to this rule, a compound that fulfils at least four of the five characteristics (Lipinski's RO5) could show ideal drug candidates. The drug-likeness properties of the top three compounds, including the positive control, are listed in [Table 3](#). From the targeted compounds, only compound 123608715 followed Lipinski's rule of five. This suggested that

**Table 3.** Drug-likeness properties.

Pubchem ID	Lipinski's rule of five					
	Molecular weight (g/mol)	Num. of H-bond acceptors	Num. of H-bond donor	log P	PSA (Å <sup>2</sup> )	Lipinski's RO5 violations
CID153012995	649.56	15	3	1.36	234.84	3
CID12149203	601.54	11	1	3.03	166.11	3
CID123608715	471.45	8	1	2.51	105.67	0
CID392622 (Control)	720.94	7	4	5.04	202.26	3

compound 123608715 could be easily absorbed in the human compared with other selected compounds. Although predicted in low bioavailability, other compounds could be potential drugs to treat SARS-CoV-2 targeting PLpro because their results of Lipinski's rule were similar with the control compound (Lipinski's RO5 violations = 3). Hence, all selected compounds were used for further analysis using all-atom MD simulation to know their stability in solvent water.

### MD analysis

From the finding of molecular docking provided in Figure 2, the potent antiviral drugs in 3 complexes may become potential inhibitors against SARS-CoV-2 due to their binding site to the catalytic site of the PLpro. To confirm the structural stability of those complexes in water solvent, all-atom MD simulation was performed [55,67–69]. The protein-ligand model for each complex for MD simulation is shown in Figure 4. Because of the slight difference of ligands' structures, we determined the box sizes, the number of counter ions and water molecules for each complex listed in Table 4.

To confirm the stable structure of the 3 complexes in water solvent, several validation parameters, including root mean square deviation (RMSD), radius of gyration (Rg), root mean square fluctuation (RMSF), solvent-accessible surface area (SASA), hydrogen bond, and total energy were analysed for each complex. In Figure 5(a), RMSD value as a function of MD time is presented. RMSD was estimated from the trajectories of MD simulations according to the Equation (1). As shown from this figure, complexes 1 and 2 involved small fluctuations at 75–80 ns and 25–75 ns, but after this time, the RMSD became stable until the end of the simulation. For model 3, small fluctuations were observed at the end of the simulation at 210–250 ns. Meanwhile, in control, small fluctuations were viewed at the initial simulation at 0–47 ns. The small fluctuation during MD simulation could occur since each residue's interactions, which includes electrostatic interaction, hydrogen bond, hydrophobic interactions, or even water molecules, involve structural rearrangement at the protein and ligand molecule interface. As of the RMSD results, those 3 complexes and control achieved the equilibrium state after 30 ns and 50 ns, respectively. This finding indicates that our complexes were stable during the simulation, despite some fluctuation points. The change of protein and ligand size correlated with the radius of gyration (Rg). A higher Rg value denoted with the loose packaging system; meanwhile, a lower Rg corresponded to a more compacted protein and ligand formation. Rg profile of 3 complexes is presented in Figure 5(b). This figure demonstrated that no significant change of radius of gyration was observed for each complex, and the graph shapes looked similar.

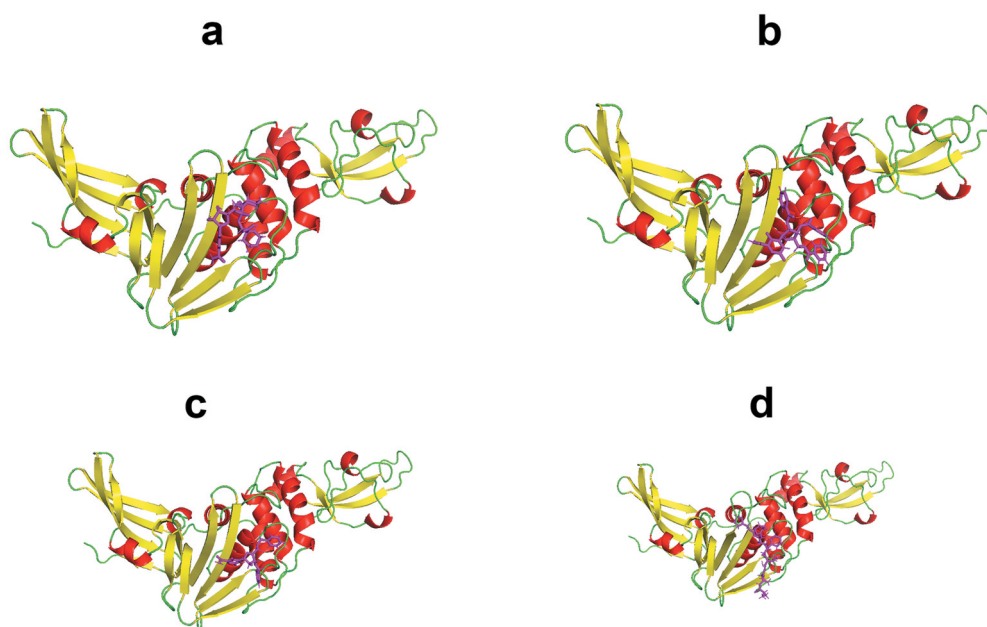


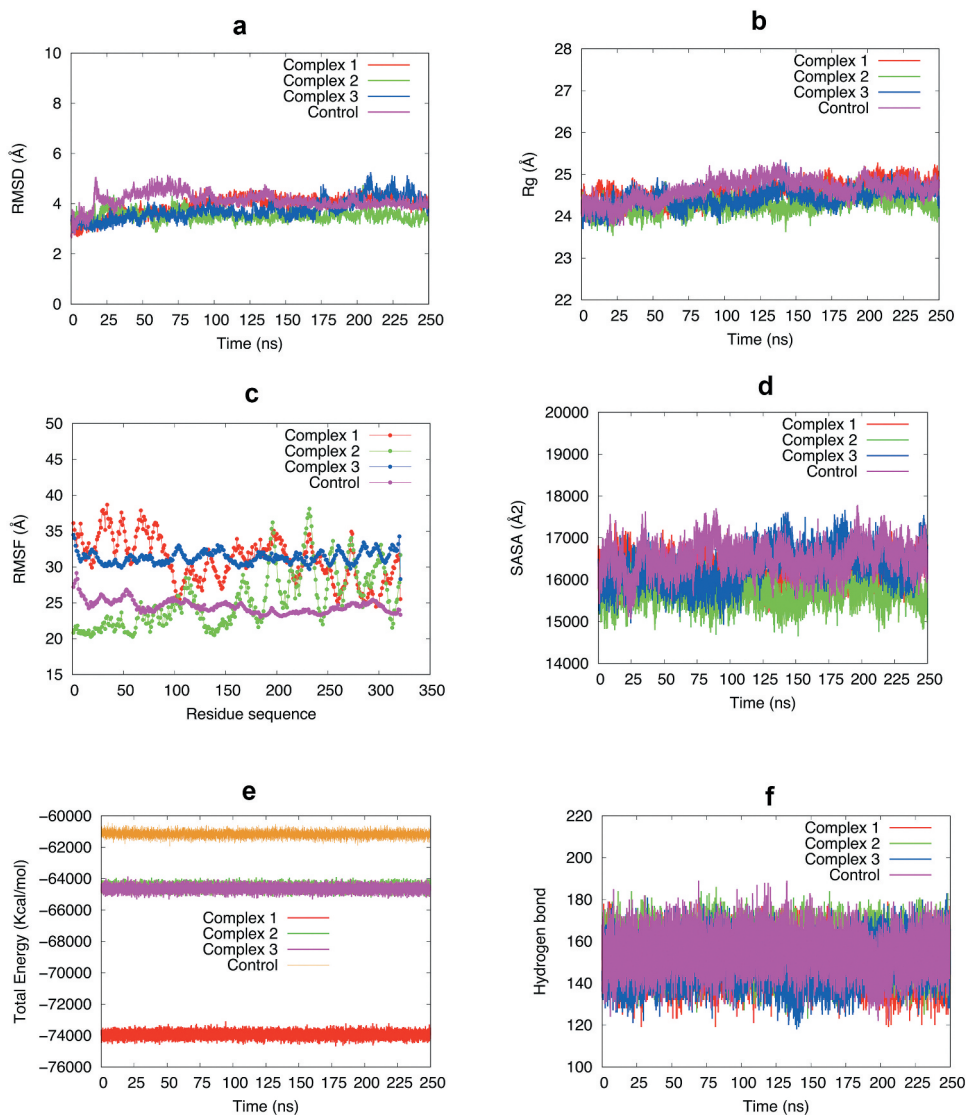
**Figure 4.** The protein-ligand model of (a) complex 1, (b) complex 2, (c) complex 3, and (d) control for MD simulation. The structures of  $\alpha$ -helix and  $\beta$ -sheet are presented by red and green colours in cartoon models, respectively. Meanwhile, the structure of ligands refers to magenta colour using stick models.

**Table 4.** Properties of MD simulation for all complexes.

Complexes	Box size ( $\text{\AA}$ )	Identities		
		No. of ions	No. of water	Total atoms
Complex 1	$75.160 \times 55.234 \times 77.526$	3 ( $\text{Cl}^-$ )	7889	28767
Complex 2	$75.160 \times 54.652 \times 77.526$	3 ( $\text{Cl}^-$ )	7707	28208
Complex 3	$75.160 \times 54.652 \times 77.526$	3 ( $\text{Cl}^-$ )	7716	28224
Control	$75.160 \times 52.617 \times 77.526$	3 ( $\text{Na}^+$ )	7190	26705

This finding suggested that no major deviation is observed, implying the complexes were in a stable state.

The flexibility over the amino acid residues for 3 complexes was determined by estimating the RMSF profile (Figure 5(c)). Most residues from complex 3 and control have lower RMSF shapes, which might be responsible for the more inflexible nature of the complex. Meanwhile, complexes 1 and 2 tend to be more flexible, as seen in the graph trends, suggesting the interaction between ligand and protein of the complex could be more easily formed because of the higher flexibility of their structure. Further, to understand the changes in protein volume for each complex, solvent-accessible surface area (SASA) was calculated. Interestingly, all complexes tend to have similar graph trends, provided in Figure 5(d). The result from the SASA profile reveals that the complex did not increase in volume during the simulation, and all complexes appeared to be stable structures. Moreover, we analysed the hydrogen bond formation of each complex

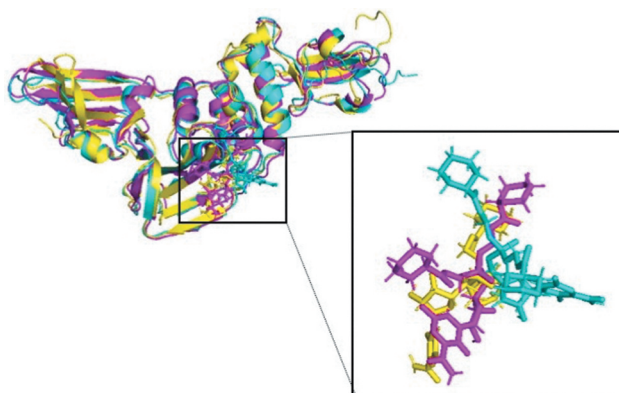


**Figure 5.** (a) RMSD value of the complexes, (b) Rg profile, (c) RMSF descriptor, (d) protein surface area measured from SASA, (e) hydrogen bond from MD trajectory, (f) total energy in the system. The complexes 1, 2, and 3 are presented by red, green, and blue colours, respectively.

because this formation involves a vital role in supporting the rigidity of a biomolecular complex. **Figure 5(e)** looked at a similar number of hydrogen bonds ranging from 120 to 180 for 3 complexes and control. Also, all complexes showed similar hydrogen profiles for the entire simulation, suggesting that the hydrogen bond formation of those complexes participated in keeping a stable complex during the simulation process. Besides, the total energy of the system was visualized to confirm the stability during the simulation (**Figure 5(f)**). In complex 1, the total energy appeared in lower energy than complexes 2

**Table 5.** The binding energy and the contribution of each energy term. The units for all contributions are in kcal/mol. Meanwhile, the standard deviation is provided in parentheses.

Complex	$E_{vdw}$	$E_{ele}$	$E_{GB}$	$E_{SA}$	$\Delta G_{MM}$	$\Delta G_{solv}^{GBSA}$	$\Delta G_{bind}$
Complex 1	-39.17 (3.50)	-19.65 (6.90)	37.07 (6.29)	-4.70 (0.38)	-58.82 (8.34)	32.37 (6.09)	-26.45 (4.07)
Complex 2	-38.27 (3.13)	-11.84 (3.75)	30.09 (3.90)	-3.90 (0.36)	-50.12 (5.07)	26.19 (3.77)	-23.92 (2.88)
Complex 3	-21.36 (3.17)	-9.73 (2.90)	21.05 (3.29)	-2.59 (0.27)	-31.09 (4.98)	18.45 (3.14)	-12.63 (2.70)
Control	-1.41 (1.44)	-230.07 (60.58)	238.54 (61.73)	-0.28 (0.35)	-231.49 (60.97)	238.25 (61.42)	6.76 (3.43)

**Figure 6.** Superimposes of the complex 1 obtained from molecular docking (yellow) and MD simulations at 150 ns (magenta) and 250 ns (cyan). Proteins and ligands are presented using cartoon and stick models, respectively.

and 3, including control. However, the total energy for all complexes did not show significant fluctuations, denoting their systems were convergence to a stable state.

To determine the top 3 compounds that have strong binding to SARS-CoV-2 PLpro compared to a control, the binding energy was calculated using the MM-GBSA method according to Equation (2). The MD trajectories were selected at the equilibrium state from 150–250 ns. Thus, 10,000 frames were utilized to estimate the binding energy of each complex. Table 5 shows the binding energy for 3 complexes and control, including the several energy contributions. The binding energy of complexes 1, 2, and 3 became -26.45 kcal/mol, -23.92 kcal/mol, and -12.63 kcal/mol, respectively. Meanwhile, the control was found to be 6.76 kcal/mol. This finding demonstrates that all complexes are in higher binding energies compared to the control and this implies that the ligands of each complex might have strong binding to the catalytic site of PLpro. We also found that complex 1 was the most stable complex due to the lowest binding energy score. Furthermore, from our results, the binding energy from the MM-GBSA method is a good agreement with our result obtained by molecular docking, where the lowest binding energy by these two methods is found in complex 1 then followed by complexes 2 and 3, and control. In addition, we observed that the  $E_{ele}$  and  $E_{GB}$  contributions for all complexes have significantly different values affecting the variation of the binding energy for each complex. These various contributions might be related to the structure of each

compound, which causes the different identities of the box size, number of ions, and number of water in the MD system. The detailed information of energy contributions for all complexes estimated by MM-GBSA is provided in Table S5.

Since complex 1 becomes the most stable structure obtained by the calculation of the binding energy using the MM-GBSA method, two snapshots of the complex from the MD trajectories at 150 ns (magenta) and 250 ns (cyan) were superimposed over the docked complex (yellow). They are presented in Figure 6. The MD structures remain in the same cavity as the docket snapshot. Also, no significant fluctuations of each protein are observed for both docked complex and MD snapshots, indicating that the protein keeps stable in the system. This finding is in good agreement with the estimation of our validation parameters (RMSD, Rg, RMSF, SASA, hydrogen bond, and total energy). Complex 1 reaches a stable structure during the simulation process. Meanwhile, in ligand molecule (stick models in the box), the structure involves the large fluctuations provided in Figure 6. These fluctuations might increase the probability of the ligand binding with the protein to form a complex structure. Therefore, the ligand (Pubchem ID: 153012995) of complex 1 may become the most promising drug against SARS-CoV-2 because it presents not only the lowest binding energy but also it participates in interactions easily to the catalytic site of SARS-CoV-2 PLpro.

## Conclusions

Inhibition of SARS-CoV-2 PLpro becomes a pivotal target for treating covid 19 due to its essential role in virus life. In this present investigation, several computational approaches such as homology modelling, molecular docking, and all-atom MD simulation were employed to search for potent drugs to inhibit PLpro. From our study, the SARS-CoV-2 PLpro model, as presented in Figure S4, was created and validated using homology modelling. Then, from molecular docking, the created PLpro model was used for receptor molecules. Meanwhile, 81 compounds retrieved from the PubChem database were used as potential antiviral drugs for treating SARS-CoV-2 and event SARS-CoV-2 mutation variants. From our results, 3 complexes having the ligands with PubChem IDs: 153012995, 12149203, and 123608715 (Figure 1) showed lower binding energies with the values of  $-6.6$ ,  $-6.6$ , and  $-6.4$  kcal/mol, respectively. These complexes demonstrate higher binding energy than Ritonavir (PubChem ID: 492405), with the binding energy of  $-5.7$  kcal/mol. This finding suggests that those 3 ligands could become promising inhibitors for SARS-CoV-2 PLpro and might easily bind to the receptor's catalytic region to make a ligand-receptor complex. Moreover, to determine the most stable structure of the 3 complexes, the binding energy was estimated using the MM-GBSA method. The binding energy of complexes 1, 2, and 3 became  $-26.45$  kcal/mol,  $-23.92$  kcal/mol, and  $-12.63$  kcal/mol, respectively. Meanwhile, the control was found to be  $6.76$  kcal/mol. These results revealed that all complexes show higher binding energies compared to the control and suggest that each complex's ligands might have strong binding to the catalytic site of PLpro. Also, complex 1 might become the most stable structure based on the lowest binding energy score around  $-26.45$  kcal/mol. Thus, two snapshot structures of complex 1 from the MD trajectories at 150 ns (magenta) and 250 ns (cyan) were superimposed over the docked complex (yellow, Figure 6). The MD structures remain in the same cavity as the docket snapshot, and no significant fluctuations of proteins are observed for both docked complex and MD snapshots. Large fluctuations



were only observed in the side chain of the ligand in MD structures. The fluctuation of the ligand might increase the probability of binding with SARS-CoV-2 PLpro.

Finally, from our investigation by computational approaches, three ligands have potential as inhibitors for SARS-CoV-2 PLpro, and the ligand of complex 1 might become the promising antiviral drug against SARS-CoV-2. Therefore, for further safety and health interest, the suggested drugs of our computational assessment need further in vitro and in vivo analysis and then, if interesting results are obtained; preclinical trials.

For future works, investigations on similar structures with existing antiviral drugs provided from Pubchem database, including Remdesivir, Galidesivir, Ribavirin, Sofosbuvir, Chloroquine, Interferon, etc. are required to find promising antiviral drugs treating SARS-CoV-2 or event SARS-CoV-2 mutation variants.

## Acknowledgements

The authors express thanks to the computational laboratory of Department of Chemistry, Hasanuddin University, for computational supports to work on this research.

## Disclosure statement

No potential conflict of interest was reported by the author(s).

## ORCID

A. Arwansyah  <http://orcid.org/0000-0003-1784-5942>

A.R. Arif  <http://orcid.org/0000-0001-8722-2949>

I. Ramli  <http://orcid.org/0000-0002-6805-4959>

I. Kurniawan  <http://orcid.org/0000-0003-3485-3063>

S. Sukarti  <http://orcid.org/0000-0002-6512-6400>

M. Nur Alam  <http://orcid.org/0000-0002-7006-5809>

## References

- [1] World Health Organization, *World covid19 report*, 2021. Available at <https://covid19.who.int/>.
- [2] J. Zhang, K. Yan, H. Ye, J. Lin, J. Zheng, and T. Cai, *SARS-CoV-2 turned positive in a discharged patient with COVID-19 arouses concern regarding the present standards for discharge*, *Int. J. Infect. Dis.* 97 (2020), pp. 212–214. doi:10.1016/j.ijid.2020.03.007.
- [3] D.S. Hui, E.I. Azhar, T.A. Madani, F. Ntoumi, R. Kock, O. Dar, G. Ippolito, T.D. Mchugh, Z. A. Memish, C. Drosten, A. Zumla, and E. Petersen, *The continuing 2019-nCoV epidemic threat of novel coronaviruses to global health — The latest 2019 novel coronavirus outbreak in Wuhan, China*, *Int. J. Infect. Dis.* 91 (2020), pp. 264–266. doi:10.1016/j.ijid.2020.01.009.
- [4] G. Tan, X. Lian, Z. Zhu, Z. Wang, F. Huang, Y. Zhang, Y. Zhao, S. He, X. Wang, H. Shen, and G. Lyu, *Use of lung ultrasound to differentiate coronavirus disease 2019 (COVID-19) pneumonia from community-acquired pneumonia*, *Ultrasound Med. Biol.* 46 (2020), pp. 2651–2658. doi:10.1016/j.ultrasmedbio.2020.05.006.
- [5] S. Mongodi, A. Orlando, E. Arisi, G. Tavazzi, E. Santangelo, L. Caneva, M. Pozzi, E. Pariani, G. Bettini, G. Maggio, S. Perlini, L. Preda, G.A. Iotti, and F. Mojoli, *Lung ultrasound in patients with acute respiratory failure reduces conventional imaging and health care provider exposure to COVID-19*, *Ultrasound Med. Biol.* 46 (2020), pp. 2090–2093. doi:10.1016/j.ultrasmedbio.2020.04.033.

- [6] L. Yang, Z. Wu, X. Ren, F. Yang, G. He, J. Zhang, J. Dong, L. Sun, Y. Zhu, J. Du, S. Zhang, and Q. Jin, *Novel SARS-like betacoronaviruses in bats, China, 2011*, *Emerg. Infect. Dis.* 19 (2013), pp. 989–991. doi:10.3201/eid1906.121648.
- [7] B. Hu, X. Ge, L.-F. Wang, and Z. Shi, *Bat origin of human coronaviruses*, *Viol. J.* 12 (2015), pp. 1–10. doi:10.1186/s12985-015-0422-1.
- [8] J. Chui, F. Li, and Z.L. Shi, *Origin and evolution of pathogenic coronaviruses*, *Nat. Rev. Microbiol.* 17 (2019), pp. 181–192. doi:10.1038/s41579-018-0118-9.
- [9] S.K.P. Lau, K.S.M. Li, Y. Huang, C.-T. Shek, H. Tse, M. Wang, G.K.Y. Choi, H. Xu, C.S.F. Lam, R. Guo, K.H. Chan, B.J. Zheng, P.C.Y. Woo, and K.Y. Yuen, *Ecoepidemiology and complete genome comparison of different strains of severe acute respiratory syndrome-related Rhinolophus bat coronavirus in China reveal bats as a reservoir for acute, self-limiting infection that allows recombination events*, *J. Virol.* 84 (2010), pp. 2808–2819. doi:10.1128/JVI.02219-09.
- [10] F. Pereira, *Evolutionary dynamics of the SARS-CoV-2 ORF8 accessory gene*, *Infect. Genet. Evol.* 85 (2020), pp. 104525. doi:10.1016/j.meegid.2020.104525.
- [11] X. Zhang, H. Cai, J. Hu, J. Lian, J. Gu, S. Zhang, C. Ye, Y. Lu, C. Jin, G. Yu, H. Jia, Y. Zhang, J. Sheng, L. Li, and Y. Yang, *Epidemiological, clinical characteristics of cases of SARS-CoV-2 infection with abnormal imaging findings*, *Int. J. Infect. Dis.* 94 (2020), pp. 81–87. doi:10.1016/j.ijid.2020.03.040.
- [12] A. Abbad, R.A.P.M. Perera, L. Anga, A. Faouzi, N.N.T. Minh, S.M.M.R. Malik, N. Iounes, A. Maaroufi, M.D. van Kerkhove, M. Peiris, and J. Nourlil, *Middle East respiratory syndrome coronavirus (MERS-CoV) neutralising antibodies in a high-risk human population, Morocco, November 2017 to January 2018*, *Euro Surveill.* 24 (2019), pp. 1–8. doi:10.2807/1560-7917.ES.2019.24.48.1900244.
- [13] H.Z. Farooq, E. Davies, S. Ahmad, N. Machin, L. Hesketh, M. Guiver, and A.J. Turner, *Middle East respiratory syndrome coronavirus (MERS-CoV) — Surveillance and testing in North England from 2012 to 2019*, *Int. J. Infect. Dis.* 93 (2020), pp. 237–244. doi:10.1016/j.ijid.2020.01.043.
- [14] A. Al-Hazmi, *Challenges presented by MERS corona virus, and SARS corona virus to global health*, *Saud. J. Biol. Sci.* 23 (2016), pp. 507–511. doi:10.1016/j.sjbs.2016.02.019.
- [15] J. Lan, J. Ge, J. Yu, S. Shan, H. Zhou, S. Fan, Q. Zhang, X. Shi, Q. Wang, L. Zhang, and X. Wang, *Structure of the SARS-CoV-2 spike receptor-binding domain bound to the ACE2 receptor*, *Nature* 581 (2020), pp. 215–220. doi:10.1038/s41586-020-2180-5.
- [16] C.W. Lu, X.F. Liu, and Z.F. Jia, *2019-nCoV transmission through the ocular surface must not be ignored*, *Lancet* 395 (2020), pp. 39. doi:10.1016/S0140-6736(20)30313-5.
- [17] X. Peng, X. Xu, Y. Li, L. Cheng, X. Zhou, and B. Ren, *Transmission routes of 2019-nCoV and controls in dental practice*, *Int. J. Oral. Sci.* 12 (2020), pp. 1–6. doi:10.1038/s41368-020-0075-9.
- [18] V. Stadnytskyi, C.E. Bax, A. Bax, and P. Anfinrud, *The airborne lifetime of small speech droplets and their potential importance in SARS-CoV-2 transmission*, *Proc. Natl. Acad. Sci. U.S.A.* 117 (2020), pp. 11875–11877. doi:10.1073/pnas.2006874117.
- [19] P. Bahl, C. Doolan, C. de Silva, A.A. Chughtai, L. Bourouiba, and C.R. MacIntyre, *Airborne or droplet precautions for health workers treating coronavirus disease 2019? J. Infect. Dis.* 189 (2020), pp. 1–29.
- [20] Y. Liu, Z. Ning, Y. Chen, M. Guo, Y. Liu, N.K. Gali, L. Sun, Y. Duan, J. Cai, D. Westerdahl, X. Liu, K. F. Ho, H. Kan, Q. Fu, and K. Lan, *Aerodynamic characteristics and RNA concentration of SARS-CoV-2 aerosol in Wuhan hospitals during COVID-19 outbreak*, *Nature* 582 (2020), pp. 557–560. doi:10.1038/s41586-020-2271-3.
- [21] M. Schwarzingler, V. Watson, P. Arwidson, F. Alla, and S. Luchini, *COVID-19 vaccine hesitancy in a representative working-age population in France: A survey experiment based on vaccine characteristics*, *Lancet Pub. Heal.* 2667 (2021), pp. 1–12.
- [22] F.P. Polack, S.J. Thomas, N. Kitchin, J. Absalon, A. Gurtman, S. Lockhart, J.L. Perez, G. Pérez Marc, E.D. Moreira, C. Zerbini, R. Bailey, K.A. Swanson, S. Roychoudhury, K. Koury, P. Li, W. V. Kalina, D. Cooper, R.W. Frenck Jr., L.L. Hammitt, Ö. Türeci, H. Nell, A. Schaefer, S. Ünal, D. B. Tresnan, S. Mather, P.R. Dormitzer, U. Şahin, K.U. Jansen, and W.C. Gruber, *Safety and efficacy of the BNT162b2 mRNA Covid-19 vaccine*, *N. Engl. J. Med.* 383 (2020), pp. 2603–2615. doi:10.1056/NEJMoa2034577.

- [23] J.H. Kim, F. Marks, and J.D. Clemens, *Looking beyond COVID-19 vaccine phase 3 trials*, Nat. Med. 27 (2021), pp. 205–211. doi:10.1038/s41591-021-01230-y.
- [24] W. Markland, T.J. McQuaid, J. Jain, and A.D. Kwong, *Broad-spectrum antiviral activity of the IMP dehydrogenase inhibitor VX-497: A comparison with ribavirin and demonstration of antiviral additivity with alpha interferon*, Antimicrob. Agents Chemother. 44 (2000), pp. 859–866. doi:10.1128/AAC.44.4.859-866.2000.
- [25] M. Wang, R. Cao, L. Zhang, X. Yang, J. Liu, M. Xu, Z. Shi, Z. Hu, W. Zhong, and G. Xiao, *Remdesivir and chloroquine effectively inhibit the recently emerged novel coronavirus (2019-nCoV) in vitro*, Cell Res. 30 (2020), pp. 269–271. doi:10.1038/s41422-020-0282-0.
- [26] P.L. Yang, M. Gao, K. Lin, Q. Liu, and V.A. Villareal, *Anti-HCV drugs in the pipeline*, Curr. Opin. Virol. 1 (2011), pp. 607–616. doi:10.1016/j.coviro.2011.10.019.
- [27] A.K. Singh, A. Singh, R. Singh, and A. Misra, *Remdesivir in COVID-19: A critical review of pharmacology, pre-clinical and clinical studies*, Diabetes Metab. Syndr. 14 (2020), pp. 641–648. doi:10.1016/j.dsx.2020.05.018.
- [28] N. Narayanan and D.T. Nair, *Ritonavir may inhibit exoribonuclease activity of nsp14 from the SARS-CoV-2 virus and potentiate the activity of chain terminating drugs*, Int. J. Biol. Macromol. 168 (2021), pp. 272–278. doi:10.1016/j.ijbiomac.2020.12.038.
- [29] C.J. Gordon, E.P. Tchesnokov, E. Woolner, J.K. Perry, J.Y. Feng, D.P. Porter, and M. Götte, *Remdesivir is a direct-acting antiviral that inhibits RNA-dependent RNA polymerase from severe acute respiratory syndrome coronavirus 2 with high potency*, J. Biol. Chem. 295 (2020), pp. 6785–6797. doi:10.1074/jbc.RA120.013679.
- [30] J. Huang, W. Song, H. Huang, and Q. Sun, *Pharmacological therapeutics targeting RNA-dependent RNA polymerase, proteinase and spike protein: From mechanistic studies to clinical trials for COVID-19*, J. Clin. Med. 9 (2020), pp. 1131. doi:10.3390/jcm9041131.
- [31] S. Ullrich and C. Nitsche, *The SARS-CoV-2 main protease as drug target*, Bioorg. Med. Chem. Lett. 30 (2020), pp. 127377. doi:10.1016/j.bmcl.2020.127377.
- [32] S. Chakraborty, *Evolutionary and structural analysis elucidates mutations on SARS-CoV2 spike protein with altered human ACE2 binding affinity*, Biochem. Biophys. Res. Commun. 538 (2021), pp. 97–103. doi:10.1016/j.bbrc.2021.01.035.
- [33] J. Osipiuk, S.A. Azizi, S. Dvorkin, M. Endres, R. Jedrzejczak, K.A. Jones, S. Kang, R.S. Kathayat, Y. Kim, V.G. Lisnyak, S.L. Maki, V. Nicolaescu, C.A. Taylor, C. Tesar, Y.A. Zhang, Z. Zhou, G. Randall, K. Michalska, S.A. Snyder, B.C. Dickinson, and A. Joachimiak, *Structure of papain-like protease from SARS-CoV-2 and its complexes with non-covalent inhibitors*, Nat. Commun. 12 (2021), pp. 743. doi:10.1038/s41467-021-21060-3.
- [34] D. Shin, R. Mukherjee, D. Grewe, D. Bojkova, K. Baek, A. Bhattacharya, L. Schulz, M. Widera, A. R. Mehdipour, G. Tascher, P.P. Geurink, A. Wilhelm, G.J. van der Heden van Noort, H. Ovaa, S. Muller, K.P. Knobloch, K. Rajalingam, B.A. Schulman, J. Cinatl, G. Hummer, S. Ciesek, and I. Dikic, *Papain-like protease regulates SARS-CoV-2 viral spread and innate immunity*, Nature 587 (2020), pp. 657–662. doi:10.1038/s41586-020-2601-5.
- [35] W. Rut, Z. Lv, M. Zmudzinski, S. Patchett, D. Nayak, S.J. Snipas, F.E. Oualid, T.T. Huang, M. Bekes, M. Drag, and S.K. Olsen, *Activity profiling and crystal structures of inhibitor-bound SARS-CoV-2 papain-like protease: A framework for anti-COVID-19 drug design*, Sci. Adv. 6 (2020), pp. 1–12. doi:10.1126/sciadv.abd4596.
- [36] R. Arya, A. Das, V. Prashar, and M. Kumar, *Potential inhibitors against papain-like protease of novel coronavirus (SARS-CoV-2) from FDA approved drugs*, preprint (2020), to appear in Cambridge Open Engage. Available at <https://chemrxiv.org/engage/chemrxiv/article/details/60c74880bdbb893898a38f6>.
- [37] B.T. Freitas, I.A. Durie, J. Murray, J.E. Longo, H.C. Miller, D. Crich, R.J. Hogan, R.A. Tripp, and S. D. Pegan, *Characterization and noncovalent inhibition of the deubiquitinase and deISGylase activity of SARS-CoV-2 papain-like protease*, ACS Infect. Dis. 6 (2020), pp. 2099–2109. doi:10.1021/acscinfecdis.0c00168.
- [38] M.W. Hull and J.S.G. Montaner, *Ritonavir-boosted protease inhibitors in HIV therapy*, Ann. Med. 43 (2011), pp. 375–388. doi:10.3109/07853890.2011.572905.

- [39] K. Uzunova, E. Filipova, V. Pavlova, and T. Vekov, *Insights into antiviral mechanisms of remdesivir, lopinavir/ritonavir and chloroquine/hydroxychloroquine affecting the new SARS-CoV-2*, Biomed. Pharmacother. 131 (2020), pp. 110668. doi:10.1016/j.biopha.2020.110668.
- [40] X. Gao, B. Qin, P. Chen, K. Zhu, P. Hou, J.A. Wojdyla, M. Wang, and S. Cui, *Crystal structure of SARS-CoV-2 papain-like protease*, Acta Pharm. Sin. B 11 (2021), pp. 237–245. doi:10.1016/j.apsb.2020.08.014.
- [41] D. Li, J. Luan, and L. Zhang, *Molecular docking of potential SARS-CoV-2 papain-like protease inhibitors*, Biochem. Biophys. Res. Commun. 538 (2020), pp. 72–79. doi:10.1016/j.bbrc.2020.11.083.
- [42] J.M. Blaney and J.S. Dixon, *A good ligand is hard to find: Automated docking methods*, Perspect. Drug. Discov. Des. 1 (1993), pp. 301–319. doi:10.1007/BF02174531.
- [43] C.A. Baxter, C.W. Murray, B. Waszkowycz, J. Li, R.A. Sykes, R.G.A. Bone, T.D.J. Perkins, and W. Wylie, *New approach to molecular docking and its application to virtual screening of chemical databases*, J. Chem. Inform. Comput. Sci. 40 (2000), pp. 254–262. doi:10.1021/ci990440d.
- [44] D.B. Kitchen, H. Decornez, J.R. Furr, and J. Bajorath, *Docking and scoring in virtual screening for drug discovery: Methods and applications*, Nat. Rev. Drug Discov. 3 (2004), pp. 935–949. doi:10.1038/nrd1549.
- [45] S.O. Aftab, M.Z. Ghouri, M.U. Masood, Z. Haider, Z. Khan, A. Ahmad, and N. Munawar, *Analysis of SARS-CoV-2 RNA-dependent RNA polymerase as a potential therapeutic drug target using a computational approach*, J. Transl. Med. 18 (2020), pp. 275. doi:10.1186/s12967-020-02439-0.
- [46] S. Sarkar, S. Gupta, W. Chakraborty, S. Senapati, and R. Gachhui, *Homology modeling, molecular docking and molecular dynamics studies of the catalytic domain of chitin deacetylase from Cryptococcus laurentii strain RY1*, Int. J. Biol. Macromol. 104 (2017), pp. 1682–1691. doi:10.1016/j.ijbiomac.2017.03.057.
- [47] M.A. Azam, S. Jupudi, N. Saha, and R.K. Paul, *Combining molecular docking and molecular dynamics studies for modelling Staphylococcus aureus MurD inhibitory activity*, SAR QSAR Environ. Res. 30 (2019), pp. 1–20. doi:10.1080/1062936X.2018.1539034.
- [48] A.A. Elfiky and A.M. Ismail, *Molecular docking revealed the binding of nucleotide/side inhibitors to Zika viral polymerase solved structures*, SAR QSAR Environ. Res. 29 (2018), pp. 409–418. doi:10.1080/1062936X.2018.1454981.
- [49] A. Fiser and A. Šali, *MODELLER: Generation and refinement of homology-based protein structure models*, Meth. Enzymol. 374 (2003), pp. 461–491.
- [50] O. Trott and A.J. Olson, *AutoDock Vina: Improving the speed and accuracy of docking with a new scoring function, efficient optimization, and multithreading*, J. Comput. Chem. 31 (2010), pp. 455–461.
- [51] N.M. O'Boyle, M. Banck, C.A. James, C. Morley, T. Vandermeersch, and G.R. Hutchison, *Open Babel: An open chemical toolbox*, J. Cheminform. 3 (2011), pp. 33. doi:10.1186/1758-2946-3-33.
- [52] G. Morris, R. Huey, W. Linkstrom, M. Sanner, R. Belew, D. Goodsell, and A. Olson, *AutoDock4 and AutoDockTools4: Automated docking with selective receptor flexibility*, J. Comput. Chem. 30 (2009), pp. 2785–2791. doi:10.1002/jcc.21256.
- [53] A. Arwansyah, A.R. Arif, G. Syahputra, S. Sukarti, and I. Kurniawan, *Theoretical studies of thiazolyl-pyrazoline derivatives as promising drugs against malaria by QSAR modelling combined with molecular docking and molecular dynamics simulation*, Mol. Simul. 47 (2021), pp. 988–1001.
- [54] T. Sumaryada, A. Arwansyah, W. Roslia, L. Ambarsari, and A. Kartono, *Molecular docking simulation of mangostin derivatives and curcuminoid on maltase- glucoamylase target for searching anti-diabetes drug candidates*, Int. Conf. Bioinform. Biomed. Eng. (2016), pp. 1–4. (<https://ieeexplore.ieee.org/document/7869832>).
- [55] R. Salomon-Ferrer, D.A. Case, and R.C. Walker, *An overview of the Amber biomolecular simulation package*, Wiley Interdiscip. Rev. Comput. Mol. Sci. 3 (2013), pp. 198–210. doi:10.1002/wcms.1121.

- [56] W.L. Jorgensen, J. Chandrasekhar, J.D. Madura, R.W. Impey, and M.L. Klein, *Comparison of simple potential functions for simulating liquid water*, *J. Chem. Phys.* 79 (1983), pp. 926–935. doi:10.1063/1.445869.
- [57] J. Wang, R.M. Wolf, J.W. Caldwell, P.A. Kollman, and D.A. Case, *Development and testing of a general Amber force field*, *J. Comput. Chem.* 25 (2004), pp. 1157–1174. doi:10.1002/jcc.20035.
- [58] J.A. Maier, C. Martinez, K. Kasavajhala, L. Wickstrom, K.E. Hauser, and C. Simmerling, *ff14SB: Improving the Accuracy of protein side chain and backbone parameters from ff99SB*, *J. Chem. Theory Comput.* 11 (2015), pp. 3696–3713. doi:10.1021/acs.jctc.5b00255.
- [59] U. Essmann, L. Perera, M.L. Berkowitz, T. Darden, H. Lee, and L.G. Pedersen, *A smooth particle mesh Ewald method*, *J. Chem. Phys.* 103 (1995), pp. 8577–8593. doi:10.1063/1.470117.
- [60] J.-P. Ryckaert, G. Ciccotti, and H.J.C. Berendsen, *Numerical integration of the cartesian equations of motion of a system with constraints: Molecular dynamics of n-alkanes*, *J. Comput. Phys.* 23 (1977), pp. 327–341. doi:10.1016/0021-9991(77)90098-5.
- [61] R.J. Loncharich, B.R. Brooks, and R.W. Pastor, *Langevin dynamics of peptides: The frictional dependence of isomerization rates of N-acetylalanyl-N-methylamide*, *Biopolymers* 32 (1992), pp. 523–535. doi:10.1002/bip.360320508.
- [62] D.R. Roe and T.E. Cheatham, *PTRAJ and CPPTRAJ: Software for processing and analysis of molecular dynamics trajectory data*, *J. Chem. Theory Comput.* 9 (2013), pp. 3084–3095. doi:10.1021/ct400341p.
- [63] B.R. Miller, T.D. Mcgee, J.M. Swails, N. Homeyer, H. Gohlke, and A.E. Roitberg, *MMPBSA.py: An efficient program for end-state free energy calculations*, *J. Chem. Theory Comput.* 8 (2012), pp. 3314–3321. doi:10.1021/ct300418h.
- [64] S. Salentin, S. Schreiber, V.J. Haupt, M.F. Adasme, and M. Schroeder, *PLIP: Fully automated protein-ligand interaction profiler*, *Nucleic Acids Res.* 43 (2015), pp. 443–447. doi:10.1093/nar/gkv315.
- [65] W.L. DeLano, *The PyMOL molecular graphics system, Version 2.3, 2020*; software available at <https://pymol.org/>.
- [66] A.C. Wallace, R.A. Laskowski, and J.M. Thornton, *Ligplot: A program to generate schematic diagrams of protein-ligand interactions*, *Protein Eng.* 8 (1995), pp. 127–134. doi:10.1093/protein/8.2.127.
- [67] S. Nakagawa, I. Kurniawan, K. Kodama, M.S. Arwansyah, K. Kawaguchi, and H. Nagao, *Theoretical study on interaction of cytochrome f and plastocyanin complex by a simple coarse-grained model with molecular crowding effect*, *Mol. Phys.* 116 (2018), pp. 666–677. doi:10.1080/00268976.2017.1406160.
- [68] K. Kawaguchi, M.S. Arwansyah, T. Kataoka, and H. Nagao, *Theoretical study of conformational transition of CDK4 by association of cyclin D3*, *Mol. Phys.* 117 (2019), pp. 2355–2361. doi:10.1080/00268976.2018.1563725.
- [69] K. Kawaguchi, S. Nakagawa, I. Kurniawan, K. Kodama, M.S. Arwansyah, and H. Nagao, *A coarse-grained model of the effective interaction for charged amino acid residues and its application to formation of GCN4-pLI tetramer*, *Mol. Phys.* 116 (2018), pp. 649–657. doi:10.1080/00268976.2017.1393574.